



**HAL**  
open science

## Ironing Out Fe Residence Time in the Dynamic Upper Ocean

E. Black, S. Kienast, N. Lemaitre, P. Lam, R. Anderson, H el ene Planquette,  
Fr ed eric Planchon, K. Buesseler

► **To cite this version:**

E. Black, S. Kienast, N. Lemaitre, P. Lam, R. Anderson, et al.. Ironing Out Fe Residence Time in the Dynamic Upper Ocean. *Global Biogeochemical Cycles*, 2020, 34 (9), pp.e2020GB006592. 10.1029/2020GB006592 . hal-02975939

**HAL Id: hal-02975939**

**<https://hal.univ-brest.fr/hal-02975939>**

Submitted on 25 Oct 2020

**HAL** is a multi-disciplinary open access archive for the deposit and dissemination of scientific research documents, whether they are published or not. The documents may come from teaching and research institutions in France or abroad, or from public or private research centers.

L'archive ouverte pluridisciplinaire **HAL**, est destin ee au d ep ot et  a la diffusion de documents scientifiques de niveau recherche, publi es ou non,  emanant des  tablissements d'enseignement et de recherche fran ais ou  trangers, des laboratoires publics ou priv es.



Distributed under a Creative Commons Attribution - NoDerivatives 4.0 International License

# Global Biogeochemical Cycles

## RESEARCH ARTICLE

10.1029/2020GB006592

### Key Points:

- The majority of the residence times determined for total Fe in the upper 250 m fall between 10 and 100 days
- Export-based results suggest that dissolved Fe cycles sub-annually to annually in the upper ocean, typically faster than previously thought

### Supporting Information:

- Supporting Information S1
- Table S1

### Correspondence to:

E. E. Black,  
erinb@ldeo.columbia.edu

### Citation:

Black, E. E., Kienast, S. S., Lemaitre, N., Lam, P. J., Anderson, R. F., Planquette, H., et al. (2020). Ironing out Fe residence time in the dynamic upper ocean. *Global Biogeochemical Cycles*, 34, e2020GB006592. <https://doi.org/10.1029/2020GB006592>

Received 27 FEB 2020

Accepted 18 AUG 2020

Accepted article online 26 AUG 2020

### Author Contributions:

**Formal analysis:** E. E. Black

**Funding acquisition:** P. J. Lam, H. Planquette, F. Planchon, K. O. Buesseler

**Investigation:** E. E. Black, N. Lemaitre

**Project administration:** P. J. Lam, K. O. Buesseler

**Resources:** P. J. Lam, H. Planquette, F. Planchon, K. O. Buesseler









**Writing - original draft:** E. E. Black, S. S. Kienast

**Writing - review & editing:** N. Lemaitre, P. J. Lam, R. F. Anderson, H. Planquette, F. Planchon, K. O. Buesseler

©2020. The Authors.

This is an open access article under the terms of the Creative Commons Attribution License, which permits use, distribution and reproduction in any medium, provided the original work is properly cited.

## Ironing Out Fe Residence Time in the Dynamic Upper Ocean

E. E. Black<sup>1,2,3</sup> , S. S. Kienast<sup>2</sup> , N. Lemaitre<sup>4</sup> , P. J. Lam<sup>5</sup> , R. F. Anderson<sup>3</sup> , H. Planquette<sup>6</sup> , F. Planchon<sup>6</sup> , and K. O. Buesseler<sup>1</sup> 

<sup>1</sup>Department of Marine Chemistry and Geochemistry, Woods Hole Oceanographic Institution, Woods Hole, MA, USA, <sup>2</sup>Department of Oceanography, Dalhousie University, Halifax, NS, Canada, <sup>3</sup>Division of Geochemistry, Lamont Doherty Earth Observatory, Palisades, NY, USA, <sup>4</sup>Department of Earth Sciences, Institute of Geochemistry and Petrology, Zürich, Switzerland, <sup>5</sup>Department of Ocean Sciences, University of California, Santa Cruz, CA, USA, <sup>6</sup>Univ Brest, CNRS, IRD, Ifremer, LEMAR, Plouzané, France

**Abstract** Although iron availability has been shown to limit ocean productivity and influence marine carbon cycling, the rates of processes driving iron's removal and retention in the upper ocean are poorly constrained. Using <sup>234</sup>Th- and sediment-trap data, most of which were collected through international GEOTRACES efforts, we perform an unprecedented observation-based assessment of iron export from and residence time in the upper ocean. The majority of these new residence time estimates for total iron in the surface ocean (0–250 m) fall between 10 and 100 days. The upper ocean residence time of dissolved iron, on the other hand, varies and cycles on sub-annual to annual timescales. Collectively, these residence times are shorter than previously thought, and the rates and timescales presented here will contribute to ongoing efforts to integrate iron into global biogeochemical models predicting climate and carbon dioxide sequestration in the ocean in the 21st century and beyond.

**Plain Language Summary** Iron is a key micronutrient for organisms living in the upper ocean, and thus, its availability is one of the key factors controlling the removal of carbon dioxide via phytoplankton growth in much of the global ocean. Until very recently, measurements of internal iron cycling were scarce. This includes estimates of how much iron leaves the surface ocean via sinking particles. Due to the lack of observations, models struggle to reproduce observed patterns in global surface iron distributions. For the first time, we constrain the rate of iron loss from the upper ocean along three basin-wide transects and bring together all preexisting estimates to determine the timescales on which different forms of iron are retained in the upper ocean. Overall, our findings suggest that iron cycles more rapidly between the surface and the subsurface ocean than previously estimated, and we encourage the modeling community to utilize the wealth of data presented here to explore the global consequences of these findings.

## 1. Introduction

Iron (Fe) is vital to the metabolic functions of many marine organisms, and its low abundance is thought to limit primary productivity throughout much of the ocean (Martin et al., 1994; Moore et al., 2013). Changes in Fe supply likely played an important role in regulating marine productivity and global climate during prior glacial-interglacial cycles (Martinez-García et al., 2014; Watson et al., 2000). Despite this important role, measurements of internal Fe fluxes (e.g., biological uptake, scavenging, and surface export) are scarce and as noted within the global modeling community, “at present, there is low confidence in model projections of how modulations to climate will affect Fe supply to the upper ocean, as models generally show poor skill and substantial disagreement in their representation of the present-day ocean iron cycle” (Tagliabue et al., 2016, 2019).

One of the most biologically active regions of the ocean is the euphotic zone, where phytoplankton drive global marine productivity and set the ocean's potential for carbon uptake via the biological pump (Ducklow et al., 2001; Knox & McElroy, 1984; Volk & Hoffert, 1985). In this zone and within the seasonally overturned waters below it (defined broadly as 0–250 m), it is thought that organisms have adapted cellular and community-level mechanisms to prevent this essential micronutrient from sinking below the winter mixed layer (Boiteau et al., 2016), where it will not be accessible again for hundreds of years (Primeau, 2005).

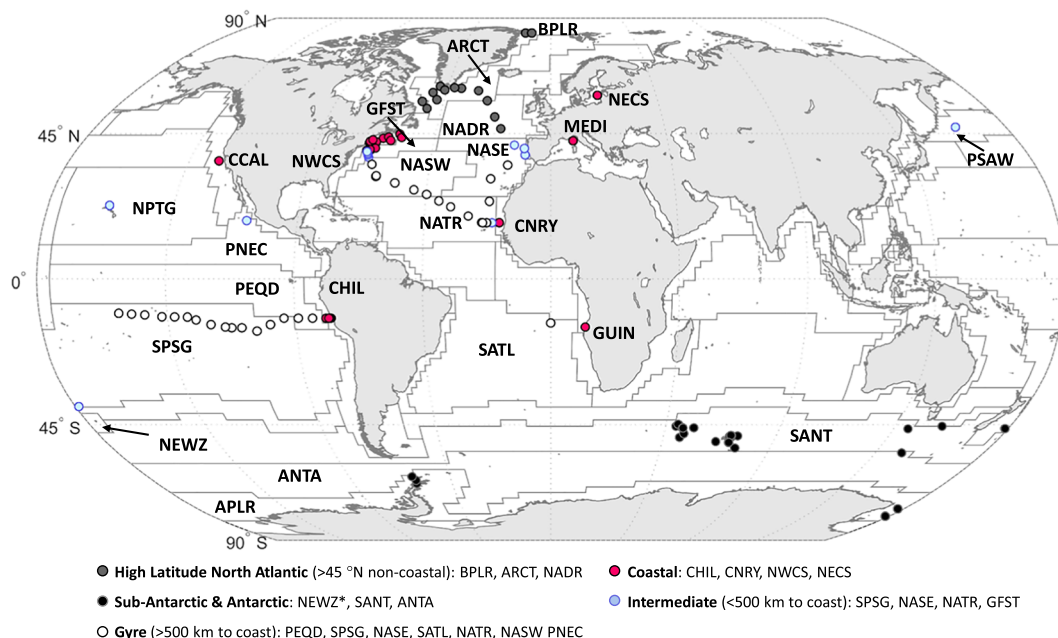


**Figure 1.** Location of upper ocean iron export studies. Study sites with reported  $F_{tot}$  are color-coded based on zones determined using distance-to-coast, latitude, and the outlined biogeochemical Longhurst Provinces (Longhurst, 2007). All Longhurst Provinces containing at least one  $F_{tot}$  are indicated with initials. The zones are described and the Longhurst Provinces they contain are listed in the legend. This study has added new  $F_{tot}$  across GEOTRACES transects in the South Pacific and the Central and North Atlantic. \*NEWZ is a coastal province, but the NEWZ locations from Frew et al. (2006) are on the transient boundary between NEWZ and SANT and displayed characteristics of SANT.

Therefore, if we are to better elucidate the processes that control carbon sequestration, we must first constrain the rates of Fe loss and retention in the surface ocean.

The residence time ( $\tau$ ) of any element, such as Fe, is equal to its inventory in a reservoir divided by the flux of this constituent into or out of this reservoir as controlled by one or more processes:

$$\tau = \frac{\text{inventory}}{\text{outputs or inputs}}, \quad (1)$$

assuming that both parameters represent quasi-steady state conditions over the timescale of  $\tau$  (inputs = outputs). How rapidly all Fe (i.e., total Fe,  $tot$ ) cycles with respect to an input or output ( $\tau_{tot}$ ) can be expressed as

$$\tau_{tot} = \frac{\text{total inventory of Fe}}{\text{outputs or inputs}}. \quad (2)$$

The total inventory of Fe is composed of dissolved ( $diss$ ) and particulate Fe, the separation of which is defined operationally by what passes through a  $\sim 0.2\text{--}0.8\ \mu\text{m}$  pore-size filter. Particulate Fe can be further characterized as lithogenic (crustally derived, *lith*), authigenic (abiotically formed, *auth*), or biological (*bio*) in origin, and these forms likely have different residence times and dissolution potentials in the upper ocean. For instance, most of the particulate Fe entering the ocean via lithogenic dust is not immediately accessible to surface biota, while dissolved Fe is thought to be more readily bioavailable (Boyd et al., 2010). The residence time of dissolved Fe ( $\tau_{diss}$ ) can be determined with respect to processes that remove or add to the dissolved Fe inventory, such as biological uptake and particle scavenging.

Few estimates exist for  $\tau_{tot}$  (Buck et al., 2010; Jickells, 1999), and those for  $\tau_{diss}$  can range from days to decades in the upper ocean (e.g., Croot et al., 2004; Kadko et al., 2019). Dust-based input estimates of  $\tau_{diss}$  are the most numerous. However, dust-only studies are mostly restricted to the Atlantic Ocean (e.g., Bergquist & Boyle, 2006; Sarthou et al., 2003) and often require an assumption of dust solubility, which can vary from

near zero to >90% (Sholkovitz et al., 2012). Furthermore, continental dust, hydrothermal vents (Ardyna et al., 2019; Holmes et al., 2017), and seafloor sediments are all sources of Fe to the marine environment, and thus, all should be accounted for in input-based residence time estimates. The main output from the upper ocean is the export flux of Fe, which is dominated by its loss via sinking particles (downwelling is slow and assumed to be a negligible Fe sink). Thus, using export as the denominator in Equation 2 provides a powerful approximation of a total upper ocean  $\tau$ . Until recently, most export-based estimates of  $\tau$  came from sediment traps (Bowie et al., 2009; Frew et al., 2006; Lamborg et al., 2008), which directly measure sinking, particle-associated Fe (see supporting information Text S1 for additional details on trap-based estimates).

An alternative approach for determining  $\tau$ , highlighted in this study, is the use of the thorium-234 and uranium-238 disequilibrium method. This export-based method integrates over timescales of weeks to months and lends itself to higher resolution sampling of the surface ocean. Here we combine new  $^{234}\text{Th}$ -derived particulate Fe export estimates from three GEOTRACES transects in the Atlantic and Pacific Oceans with all prior trap and  $^{234}\text{Th}$ -based export measurements (Figure 1; see Table S1 for data compilation). Using Fe inventories that were determined quasi-simultaneously with Fe export, we derive over 100 new estimates of  $\tau_{tot}$  from the upper 250 m (see Table S2 for data compilation). We also put constraints on  $\tau_{diss}$  with respect to its removal via particle export.

## 2. Materials and Methods

### 2.1. Biogeochemical Provinces

The study sites (Table 1) are grouped geographically and according to their biogeochemical Longhurst Provinces (Longhurst, 2007). Our assessment covers bloom and non-bloom periods in the high latitude (>45°) North Atlantic or HLNA (gray, Figure 1), in the coastal waters of the Pacific and Atlantic (pink) and in the sub-Antarctic (black). Locations at low latitudes that are not classified as coastal are split into intermediate (<500 km offshore, blue) and gyre (>500 km offshore, white) regions.

### 2.2. $^{234}\text{Th}$ Analyses and the $^{238}\text{U}$ - $^{234}\text{Th}$ Disequilibrium Method

$^{234}\text{Th}$  (half-life ~ 24 days) is a highly particle reactive radioisotope, while its parent  $^{238}\text{U}$  (half-life ~ 4.5 billion years) behaves conservatively in the ocean with respect to salinity. If no processes sufficiently perturb the  $^{238}\text{U}$ - $^{234}\text{Th}$  system, the activities of the parent and daughter isotopes are equal. In the surface ocean, however,  $^{234}\text{Th}$  attached to rapidly sinking particles can leave a deficit of  $^{234}\text{Th}$  with respect to  $^{238}\text{U}$  if this process is faster than  $^{234}\text{Th}$  can be replenished by in situ  $^{238}\text{U}$  decay. The magnitude of this deficit reflects the net particulate export of  $^{234}\text{Th}$ . The total export flux of Fe ( $F_{tot}$ ) can be determined by multiplying the Fe: $^{234}\text{Th}$  ratio (moles  $\text{L}^{-1}$ :decays per minute  $\text{L}^{-1}$ ) on large or “sinking” particles (Bishop et al., 1977) at a given depth  $z$  and the integrated flux of  $^{234}\text{Th}$  at that depth.

The  $^{234}\text{Th}$  data and their collection have been described (Black et al., 2018; Lemaitre et al., 2018; Owens et al., 2015). Sinking particulate  $^{234}\text{Th}$  was collected on pre-filters, >51  $\mu\text{m}$  for U.S. GEOTRACES and >53  $\mu\text{m}$  for GEOVIDE. Total  $^{234}\text{Th}$  was collected with Niskin bottles (Pike et al., 2005). Total  $^{238}\text{U}$  was derived from salinity (Owens et al., 2011). Steady-state assumptions were made, and lateral advection of  $^{234}\text{Th}$  was determined to be negligible when these calculations were possible (e.g., along transects where a  $^{234}\text{Th}$  gradient and current speeds could be determined) or where prior studies had already indicated that these assumptions were valid (Black et al., 2019; Lemaitre et al., 2018; Owens et al., 2015). For the new locations in this study, upwelling was a significant factor for the coastal region of the Pacific campaign only, and the appropriate adjustments were made (Black et al., 2018).

### 2.3. Fe Analyses

The sample collection and analytical procedures used for particulate and dissolved Fe are detailed where they are publicly available for the U.S. GEOTRACES campaigns TN303, KN199-04, and KN204-01 (see Data Availability Statement and Text S2). In short, particulate material was collected with 51  $\mu\text{m}$  polyester mesh prefilters (>51  $\mu\text{m}$  “sinking” fraction) and 0.8  $\mu\text{m}$  polyethersulfone membrane filters (0.8–51  $\mu\text{m}$  “suspended” fraction). Dissolved Fe (<0.2  $\mu\text{m}$ ) samples were collected using either the Geofish towed system (2–3 m depth samples, Bruland et al., 2005) or Teflon-lined GO-FLO samplers deployed on the U.S. GEOTRACES clean CTD rosette (sample depths greater than ~20 m, Cutter & Bruland, 2012). The total

**Table 1**  
*<sup>234</sup>Th- and Sediment Trap-Based Iron Export Studies*

Study	Dates	<i>n</i>	General location (program)	Method	Export depths (m)	Annual Chl- <i>a</i> (mg m <sup>-3</sup> )	Prior 16-day NPP (mmolC m <sup>-2</sup> day <sup>-1</sup> )	Predicted input from dust (μmolFe m <sup>-2</sup> day <sup>-1</sup> )	Fe export (μmolFe m <sup>-2</sup> day <sup>-1</sup> )
Landing and Bruland (1987)	8/1980 to 11/1981	2	NE Pacific (VERTEX)	ST	100–250	0.2–0.6	--	0.04–0.9	0.4–3
Quétel et al. (1993)	4/1986 to 10/1987	36	Ligurian Sea (DYFAMED)	ST	200	0.3	--	3–43	0.4–62
Martin (1990)	1/1987	3	Antarctic Peninsula	ST	100	0.3–0.6	--	0.005–0.008	2–654
Schiffler et al. (1997)	8/1992 to 6/1993	13	NE Water Polynya	ST	130	0.5–0.7	--	0.1–0.4	2–16
Collier et al. (2000)	11/1996 to 12/1997	24	Ross Sea (JGOFS)	ST	200–206	0.7–5	--	0.0004–0.03	0.01–2
Smith et al. (2014)	9/1997	12	Coastal NW Atlantic	<sup>234</sup> Th	50	0.5–1.3	41–88	0.3–1.6	2–151
Weinstein and Moran (2005)	7/1999	6	Labrador Sea	<sup>234</sup> Th	50–100	0.9–1.4	37–65	0.2–0.3	3–16
Pohl et al. (2004)	12/1999 to 3/2001	47	Gotland Basin	ST	120	6	55–101 <sup>a</sup>	1–4	2–138
Stanley et al. (2004)	6/2001 to 9/2001	6	Bermuda (BATS)	ST	150–300	0.1	25–27	1–5	2–16
Frew et al. (2006)	2/2003	4	Subantarctic SE of New Zealand (FeCycle-I)	ST	80–120	0.3	90–98	0.03–0.04	0.2–0.5
Lamborg et al. (2008)	6/2004 to 8/2005	26	Hawaii (ALOHA) & Northwest Pacific (K2)	ST	150–300	0.1–0.5	52–67	0.4–2	1–10
Planquette et al. (2011)	11/2004 to 1/2005	15	Crozet Islands (CROZEX)	<sup>234</sup> Th	80–225	0.2–0.7	2–57	0.04–0.7	3–145
Bowie et al. (2009)	1/2007 to 2/2007	1	Subantarctic SW of Tasmania	ST	150	0.2–0.4	49–83	0.08–0.6	0.07–0.2
Noble et al. (2012)	11/2007	4	South Atlantic Low Oxygen Zone (CoFeMUG - GTC)	ST	60–150	0.1–4	67–91	0.2–3	0.09–0.9
Ellwood et al. (2014)	9/2008 to 10/2008	8	East of New Zealand (GTC Process FeCycle-II)	ST	100–200	0.3	30 <sup>a</sup>	0.1–0.2	5–20
This study	10/2010 to 12/2011	36	North Atlantic (GTC KN199-04 and KN204-01)	<sup>234</sup> Th	100–200	0.6–1	12–72	0.3–35	0.8–82
Bowie et al. (2015)	10/2011 to 11/2011	10	Kerguelen Plateau (GTC Process)	ST	200	0.4–0.8	5	0.1–0.5	0.2–6
Lemaître et al. (2016)	10/2011 to 11/2011	9	Kerguelen Plateau (GTC Process)	<sup>234</sup> Th	35–123	0.2–1	4	0.1–0.6	2–43
This study	10/2013 to 12/2013	39	Southeastern Pacific (GTC TN303)	<sup>234</sup> Th	100–200	0.1–9	34–188	0.006–0.9	0.4–127
This study	5/2014 to 6/2014	11	North Atlantic (GTC GEOVIDE)	<sup>234</sup> Th	40–200	0.3–1	4–146	0.2–8	1–70

*Note.* Studies conducted within the GEOTRACES program are abbreviated GTC under general location. Studies are bolded if residence times were calculable with available data (from cited references here, Croot et al., 2007; Gourain et al., 2019; Quéroué et al., 2015; or Lannuzel et al., 2011; Planquette et al., 2007; Tonnard et al., 2020). The number of individual time points (i.e., one station sampled repeatedly) and/or locations are indicated by *n*.

<sup>a</sup>This net primary production (NPP) range is limited by a lack of satellite data for the full duration of sampling and for all locations.



inventory of Fe for the upper 100 m and 200 m was determined by linearly interpolating the concentration of Fe in each size fraction at 1-m intervals (i.e., sinking, suspended, and dissolved) and summing all phases throughout a given depth region. Most particles in the 0.2 to 0.8  $\mu\text{m}$  size range are likely not captured by these sampling protocols, which were set up to optimize collection and particle distribution on 142 mm-diameter filters. Therefore, the particulate Fe inventory and resulting total Fe inventory could be slightly underestimated. Sample processing during the GEOVIDE campaign was performed similarly and in accordance with GEOTRACES recommendations (see Text S2).

Fe export fluxes ( $F$ ) were determined in this study using the  $^{238}\text{U}$ - $^{234}\text{Th}$  method, and prior estimates were compiled from studies utilizing sediment traps or the  $^{238}\text{U}$ - $^{234}\text{Th}$  method in the upper 300 m (Tables 1 and S1). Export-based residence times for prior studies were calculated where some combination of particulate and dissolved Fe inventories was available at a given location close to the sampling period of the export measurement (bolded studies, Table 1). If total Fe inventories were calculated from individual, published particulate and dissolved inventory datasets, the studies were cited in Table 1. Where sediment traps were used, the Fe inventories have been calculated from surface to the trap depth and the residence times determined accordingly. At a couple of locations (e.g., Bowie et al., 2015; Lemaitre et al., 2016), the traps were located below the inventory measurements (e.g., mixed layer inventory measured to 123 m and sediment trap deployed at 200 m), and the measured inventories were extrapolated to cover unquantified inventory gap.

It is important to note that the lateral movement of dissolved Fe over annual timescales can be an additional sink (or source) of Fe that would increase (or decrease) the calculated loss of Fe and shorten (or lengthen) the residence times calculated here. In the Peruvian coastal region, for example, an offshore flux of  $\sim 1 \mu\text{mol m}^{-2} \text{ day}^{-1}$  (adapted from Sanial et al., 2018) is not substantial compared to the  $F_{tot}$  of  $61 \mu\text{mol m}^{-2} \text{ day}^{-1}$  found in the coastal region. However, for the region just offshore ( $F_{tot}$  of  $3 \mu\text{mol m}^{-2} \text{ day}^{-1}$ ), the lateral flux is significant. Although these boundary zones are likely narrow, as evidenced by dissolved Fe concentrations rapidly decrease past shelf breaks (Bruland et al., 2005; Kudela et al., 2006), the one-dimensional determination of  $\tau_{tot}$  with respect to particulate export should be considered an upper limit (longest possible  $\tau$ ) at these coastal-intermediate boundaries, where lateral influences may be important.

## 2.4. Export Flux Composition

The different fractions of the total export flux of Fe were determined sequentially. First, the fraction of  $F_{tot}$  that could be attributed to the sinking of organic matter ( $F_{bio}$ ) was determined by multiplying the Fe:P ratio of bulk phytoplankton, commonly  $\sim 0.005 \text{ mol mol}^{-1}$  (Ohnemus et al., 2016; Twining et al., 2011; Twining & Baines, 2013), or a locally applicable ratio (Twining et al., 2004) by the flux of phosphorus measured at a given depth (see section 2.4.2). Second, the lithogenic flux of Fe ( $F_{lith}$ ) was determined by multiplying a locally derived aerosol Fe:Al (Buck et al., 2019; Gautier et al., 1990; Gunn et al., 1970; see Table S2) by the large particle concentration to activity ratio of Al: $^{234}\text{Th}$  and the  $^{234}\text{Th}$  flux at a given depth (McLennan, 2001). The North Pacific equatorial zone was the only location ( $n = 1$ ) where the average upper continental crust (UCC) ratio of 0.21  $\text{mol mol}^{-1}$  was used. Since  $F_{lith}$  was less than  $F_{tot}$  at nearly all locations (see section 2.4.1) and the observed Fe:Al on large or sinking particles was greater than the UCC or the locally derived Fe:Al (i.e., from aerosol or mineral analyses),  $F_{tot}$  generally included some fraction of Fe from biogenic and authigenic sources. In the few cases where  $F_{lith} + F_{bio}$  was greater than  $F_{tot}$ , the  $F_{lith}$  was set to  $F_{tot}$  minus  $F_{bio}$  (i.e., no  $F_{auth}$  present) and  $F_{lith}$  should be considered an upper limit. Otherwise, after  $F_{bio}$  and  $F_{lith}$  were considered, the remainder of  $F_{tot}$  was assumed to be authigenic in origin, formed by local abiotic sorption processes and/or precipitation of Fe oxyhydroxides. The sum of biogenic and authigenic Fe fluxes is calculated as  $F_{bio+auth} = F_{tot} - F_{lith}$ .  $F_{bio}$  was the first phase determined, in part, because of the variability and uncertainty associated with Fe:Al ratios. This calculation sequence guarantees that any exported phosphorus has a corresponding quantity of biological Fe associated with it, which is especially important when  $F_{bio} < F_{lith}$ .

### 2.4.1. $F_{lith}$

Because  $F_{lith}$  is a calculated quantity from Fe:Al, at some locations, the  $F_{lith}$  was greater than  $F_{tot}$ , which was directly measured. Of the  $\sim 300$   $F_{lith}$  determinations, 12% ( $n = 36$ ) were greater than  $F_{tot}$ . Most of these locations ( $n = 27$ ) were from this study's North Atlantic campaigns (GA03 and GEOVIDE), and the  $F_{lith}$  were

higher by ~20%, on average. These higher  $F_{lith}$  could be due to variability in the Fe:Al ratio from continental sources or the adsorptive scavenging of Al by biogenic particles (e.g., diatom frustules) (Barrett et al., 2018; Gehlen et al., 2002; Middag et al., 2015). When  $F_{lith}$  was greater than  $F_{tot}$  at the Atlantic locations, Fe:Al on large particles ranged from 0.21 to 0.30 mol mol<sup>-1</sup>. These values fell between the UCC average (0.21) and the local North Atlantic average aerosol Fe:Al ratio of  $0.314 \pm 0.053$  (Shelley et al., 2015). Ratios below the local average could be a result of source variability and dust that did not originate from the Sahara-Sahel region. The relative standard deviation of this Fe:Al compilation (17%), which includes direct measurements from the GA03 campaign, suggests that most of the elevated North Atlantic  $F_{lith}$  component could be attributed to ratio variability alone and that an assumed uncertainty of 20% in the  $F_{lith}$  calculations would be appropriate.

#### 2.4.2. $F_{bio}$

Non-biogenic P could be present in exported particulate material, which could overestimate  $F_{bio}$ . Phosphorus derived from crustal sources was estimated, where large particle P:Al ratios could be determined, by multiplying a P:Al ratio of 0.0076 mol mol<sup>-1</sup> by the Al export flux (Taylor & McLennan, 1995). The lithogenic P fraction was negligible compared to the total P exported at most locations (<2%) and did not impact the calculation of biological Fe export from Fe:P ratios. The maximum lithogenic P contribution to export was ~10% at a few stations in the Atlantic. To maintain consistency, the potential lithogenic P contribution was not subtracted from P export before calculating the biological export flux of Fe. It is also important to note that in some unusual instances, where Fe-oxyhydroxides are high (e.g., near the Peru margin), adsorbed PO<sub>4</sub> can also be a significant fraction of particulate P (e.g., Lam et al., 2018).

While plankton Fe:P stoichiometries of ~0.005 mol mol<sup>-1</sup> are typical, taxonomic and regional differences have been observed (Twining & Baines, 2013). We have taken a conservative approach here, using smaller Fe:P ratios and reporting the resulting lower limits of  $F_{bio}$  when applicable (see Table S1). Using prior analyses of phytoplankton functional groups (from pigment analyses) and Fe:P (from bulk particle and cellular measurements), it was determined that a Fe:P of 0.005 was appropriate for the Atlantic and Pacific locations in this study (Ohnemus et al., 2016; Twining et al., 2015). For a single study near the Crozet Islands (Planquette et al., 2011), we did not calculate  $F_{bio}$  using a Fe:P ratio. A weak acetic acid leach was used to determine  $F_{bio}$  directly. We have reported these direct estimates ( $F_{bio}:F_{tot}$  ranges from 0.02% to 0.9%) with our calculated  $F_{bio}$ , but Planquette et al. (2011) note that the absolute  $F_{bio}$  will likely be higher at this location than determined with the leaching method.

Due to the inherent assumptions in these calculations, the  $F_{bio}$  we report here should be considered in the context of broad, regional patterns. We examined  $F_{bio}$  at a total of 177 locations, including 108 locations with associated  $\tau$ . There was no difference between the average  $F_{bio}:F_{tot} \pm 1$  standard deviation (s.d.) for the 108 locations (5%  $\pm$  8%) and for all locations (4%  $\pm$  7%). While  $F_{bio}:F_{tot}$  for all locations ranged from 0.02% to 59%, the low mean indicates that the remaining flux of Fe ( $F_{lith} + F_{auth}$ ) is generally much larger than  $F_{bio}$  and local differences in Fe:P would not change the patterns observed in Fe residence times for the individual fraction of Fe.

### 2.5. Residence Times of Particulate and Dissolved Fe

Using the export fractions detailed above, we define three additional  $\tau$ , including the residence time of particulate lithogenic Fe ( $\tau_{lith}$ ):

$$\tau_{lith} = \frac{\text{particulate inventory of Fe}}{F_{lith}}, \quad (3)$$

and the upper ( $\tau_{diss,bio}$ ) and lower ( $\tau_{diss,bio+auth}$ ) bounds of the residence time of dissolved Fe ( $\tau_{diss}$ ):

$$\tau_{diss,bio} = \frac{\text{dissolved inventory}}{F_{bio}}, \quad (4)$$

$$\tau_{diss,bio+auth} = \frac{\text{dissolved inventory}}{F_{auth} + F_{bio}}. \quad (5)$$

The residence time of lithogenic Fe would ideally be defined using only the particulate lithogenic Fe inventory as the numerator in Equation 3, as it reflects the removal of the particulate lithogenic Fe inventory by

the export of lithogenic Fe. However, since the relevant measurements to determine particulate lithogenic Fe inventories are not always available and we cannot separate the different Fe fractions in these instances, we use the full particulate Fe inventory in this study and the reported  $\tau_{lith}$  should be considered an upper estimate (i.e., longer residence time). Equation 4 represents the upper limit on  $\tau_{diss}$  (longest possible  $\tau$ ) and is the residence time of dissolved Fe with respect to removal by biological uptake and export of biogenic particulate Fe. Conversely,  $\tau_{diss,bio+auth}$  is the lower limit on  $\tau_{diss}$  (shortest possible  $\tau$ ) and represents the residence time of dissolved Fe with respect to removal by biological uptake, abiotic sorption, and precipitation processes followed by the export of biogenic and authigenic particulate Fe. If authigenic Fe originated non-locally, however, this would decrease the fraction of the observed  $F_{auth}$  that is locally derived, and the true residence time would be longer.

As noted in section 2.3, the sampling procedures do not capture most small particles between 0.2 and 0.8  $\mu\text{m}$ , and both  $\tau_{lith}$  and the residence time of total Fe ( $\tau_{tot}$ ) incorporate a slightly underestimated particulate Fe inventory. For  $\tau_{lith}$ , this missing fraction is likely offset by the addition of non-lithogenic Fe in the particulate inventory described above. At locations where authigenic Fe is an important part of the inventory, the authigenic Fe will probably dwarf any Fe in the missing small particle fraction, which is why  $\tau_{lith}$  should generally be regarded as an upper estimate. While we expect the Fe in the 0.2–0.8  $\mu\text{m}$  particle fraction to be much less than the dissolved Fe and >0.8  $\mu\text{m}$  particulate Fe inventories that combine for the total Fe inventory, the underestimation could produce marginally shorter  $\tau_{tot}$ . We anticipate that this underestimation is within the current minimum uncertainty of  $\tau_{tot}$  (~10%; see Text S2).

## 2.6. Ancillary Data

Net primary production (NPP) is from Carbon-based Production Model-2 outputs (Westberry et al., 2008) derived from SeaWiFS (studies 1997 to mid-2002) or MODIS (studies after mid-2002) products. NPP was determined for the 16 days prior to sampling using a weighted average of 8-day NPP products. For trap studies where average Fe fluxes were reported for a multi-day event, the average NPP used was from 16 days prior to sampling to the last sampling day. No satellite products were available for comparison with Smith et al. (2014) and the decadal SeaWiFS average for the 16 days prior to the sampling event was used instead (1998–2007). Annual chlorophyll-a concentrations were determined with MODIS-Aqua products (0.083° resolution, 2006 to 2016).

Annual and monthly dust fluxes were provided by Albani et al. (2014) and used to determine Fe inputs to the surface ocean (Table 1). The upper continental crust concentration of Fe (3.5% by weight) (Rudnick & Gao, 2014) was multiplied by the minimum and maximum dust flux estimate for the month prior to sampling effort to determine the range in possible dust inputs of Fe predicted at a given location (0.94°N-S by 1.25°E-W resolution). When comparing Fe inputs and outputs (Table 1), it is important to note that modeled dust fluxes can be one to two orders of magnitude less than measured fluxes (Winckler et al., 2008).

## 3. Results and Discussion

### 3.1. The Residence Time of Total Iron in the Upper Ocean Is Sub-Annual

We begin with an assessment of the residence time of total iron in the upper ocean. The full range in  $\tau_{tot}$  from this study is 1 day to 2.2 years (Figure 2) and the few previous estimates of  $\tau_{tot}$  ( $n = 3$ ) fall within this range (Figure 3; Buck et al., 2010; Jickells, 1999). The median is 33 days, and the mean is 86 days. Sixty-seven percent of  $\tau_{tot}$  from this study fall in a narrow, 10- to 100-day range (bolded lines, Figure 2), shorter than most of the prior estimates of  $\tau$ , which were almost all  $\tau_{diss}$  (Figure 3). The small range of variability in  $\tau_{tot}$  is surprising considering the diversity of methods, export depths, and locations represented in this dataset (Table 1).

By consolidating these estimates, we provide ocean models with a range in rate constants for Fe removal ( $\lambda_{tot}$ ), which is defined as  $1/\tau_{tot}$ . These first order rate constants represent the result of all Fe export and retention processes in the surface ocean. The range in  $\lambda_{tot}$  observed here (0.01–1  $\text{day}^{-1}$ ) is remarkably similar to the removal rate of bulk particles assuming average settling velocities of 10 to 150  $\text{m day}^{-1}$  through the upper 250 m of the ocean (0.04–0.6  $\text{day}^{-1}$ ) (McDonnell & Buesseler, 2010). Thus,  $\lambda_{tot}$  can be used as an integrated parameter in ocean models to test the combined rates of the individual processes driving carbon uptake and Fe export in the global ocean.



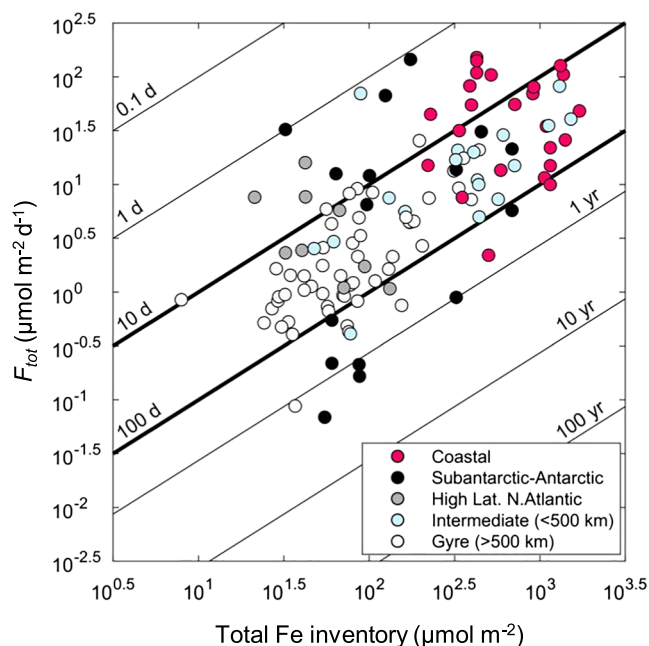


**Figure 2.** Residence times of total iron. Residence times (diagonal lines) for this study were determined using semi-simultaneously measured Fe inventories and  $F_{tot}$  at depths of 40 to 225 m. Most  $\tau_{tot}$  (67%) range from 10–100 days (bold diagonal lines), despite large differences in total Fe inventories ( $x$ -axis),  $F_{tot}$  ( $y$ -axis), predicted dust inputs (Table 1) and satellite-based NPP (Table 1).

Estimates of  $\tau_{tot}$  do not correlate strongly with source proximity (i.e., distance-to-coast,  $r^2 = 0.12$ ; Table S3) or indicators of phytoplankton biomass (i.e., Chl- $a$ ,  $r^2 = 0.14$ ; Table S3) and do not change predictably between different regions (Figure 2). In contrast, Fe inventories and  $F_{tot}$  are better correlated with each other (total inventory  $r^2 = 0.48$ , dissolved inventory  $r^2 = 0.31$ ; Figure 2), as are simultaneous measures of the export of particulate organic carbon ( $F_{POC}$ ) and  $F_{tot}$  ( $r^2 = 0.40$ ). Due to the strong link between  $F_{POC}$  and  $F_{tot}$ ,  $\tau_{tot}$  has a positive log-log relationship with  $F_{POC}$  ( $r^2 = 0.30$ ; see Table S3 and Figure S2 for additional statistics, regressions, and residual results).

A regional examination of  $\tau_{tot}$  and  $F_{tot}$  (Figure 2 and Table 2; additional details in Text S1 and Figure S3) shows that coastal locations generally have the largest inventories of Fe and large  $F_{tot}$ , due to their proximity to dust and sediment sources, while the gyre locations have lower inventories,  $F_{tot}$ , and  $F_{POC}$ . As expected, intermediate locations have results that fall in between those from the coastal and gyre regions. Considering the large range in Fe inventories,  $F_{tot}$ , Chl- $a$ , modeled dust inputs, collection methods (see Figure S4) and  $F_{POC}$  observed across these three regimes (Tables 1 and 2), as well as the absence of a single driving factor for  $\tau_{tot}$ , it is notable that the majority of  $\tau_{tot}$  are narrowly confined from 10 to 100 days.

Conversely, results from the subantarctic high nutrient-low chlorophyll (HNLC) region cover the full range of  $F_{tot}$  and  $\tau_{tot}$  (Figure 2). The HLNA and subantarctic HNLC zone are unique ocean regions

known to be seasonally or persistently iron-limited, respectively (Moore et al., 2013). Mean dissolved Fe inventories are lowest here (Table 2) and the export of Fe during short periods of intense removal (e.g., blooms) reaches rates that would be unsustainable over long periods, causing  $\tau_{tot}$  to fall to  $\sim 1$  day in locations near the Crozet Islands (data in Table S2). On the other hand,  $\tau_{tot}$  can be up to 2 years at other times or in other locations, such as the subantarctic and Antarctic waters south of Tasmania (data in Table S2). These latter situations likely represent typical, non-bloom conditions for the iron limited subantarctic region. The mean  $\tau_{tot}$  of 169 days is significantly longer here than in any other zone and is outside of the 10- to 100-day range (Table 2). In fact, two thirds of the subantarctic locations have  $\tau_{tot}$  outside of this range ( $<10$  or  $>100$  days). The extremely low Fe inventories found in these Fe-limited regions set the stage for significant swings in  $\tau_{tot}$  with even minute shifts in Fe inputs. These shifts in  $\tau_{tot}$  from days to years could reflect the response to intermittent, albeit small, Fe inputs, such as from dust or eddies (Measures & Vink, 2001), and a tight coupling of the carbon and Fe cycles in these areas.

### 3.2. Timescales of Particulate and Dissolved Iron Cycling in the Surface Ocean

The fraction of the total export flux of Fe that is made up of each component is largest for  $F_{lith}$ , on average, and smallest for  $F_{bio}$ .  $F_{tot}$  can be dominated by lithogenic Fe, even if the processes that package Fe into sinking particles are strongly influenced by the actions of surface communities and correlated with  $F_{POC}$ . This is reflected in the average  $F_{lith}$  ( $\pm$  s.d.) for all locations equaling  $66\% \pm 30\%$  of  $F_{tot}$  (range = 2–100%). It is unsurprising then that in each of the five zones the average  $\tau_{lith}$  is between 10 and 100 days, identical to the majority of the  $\tau_{tot}$  estimates (Table 2). The zonal medians are below 50 days (Table 2). At sites in the North Atlantic and South Pacific where P and Al data exist for the full particulate inventory (i.e., all particle sizes,  $n = 72$ ), we can separate the lithogenic and bio-authigenic particulate Fe inventories and compare  $\tau_{lith}$  calculated with the total particulate inventory (Equation 3) to  $\tau_{lith}$  calculated with the particulate lithogenic inventory only. The latter are 50% shorter, on average (Figure S5). Even though the  $\tau_{lith}$  calculated using only the particulate lithogenic inventory are shorter, 75% fall within 10 to 100 days, the same range as we see for  $\tau_{tot}$  and  $\tau_{lith}$  calculated using the total particulate inventory.

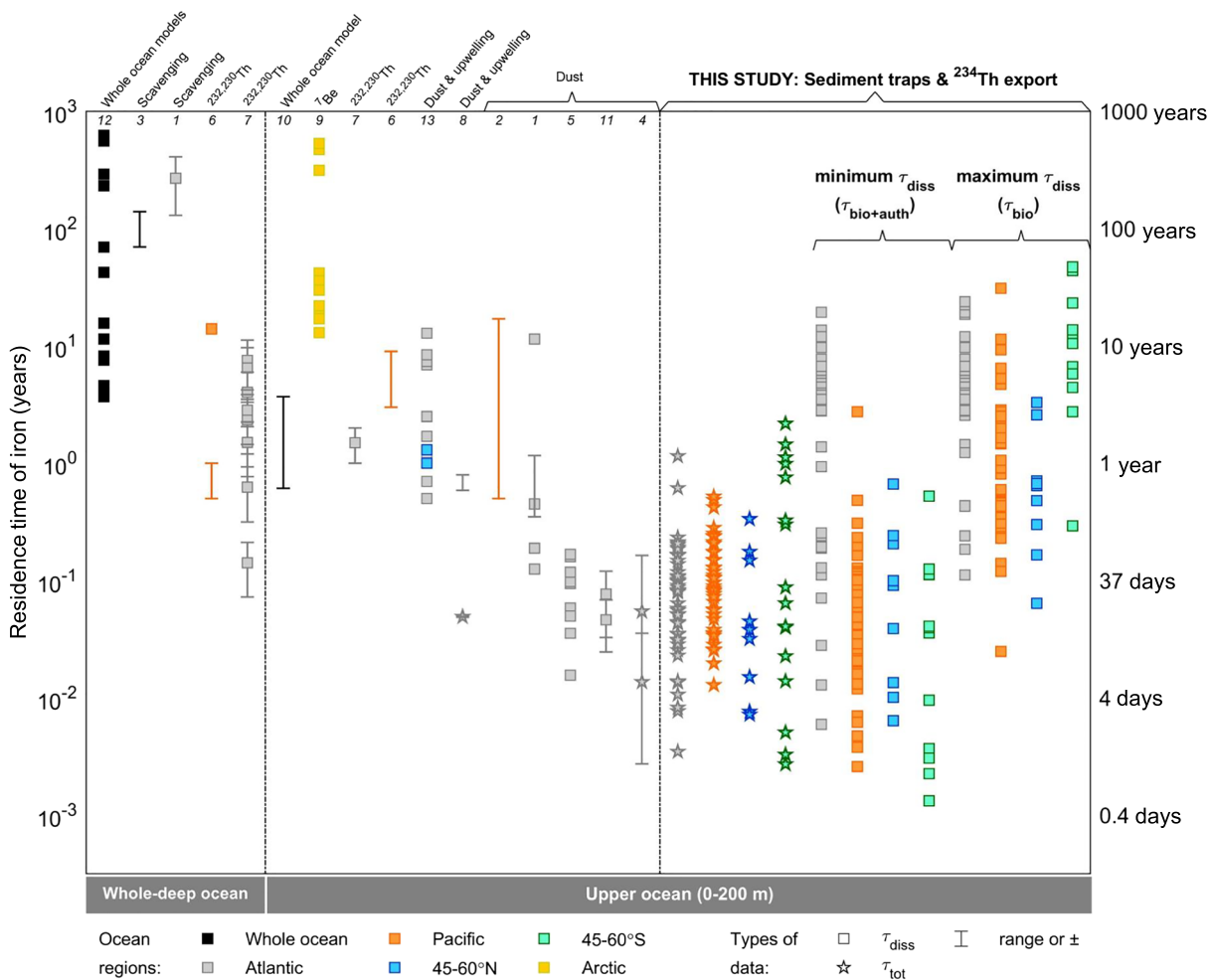


**Figure 3.** Compilation of iron residence times in the global ocean. Each symbol represents an estimate from a unique location or a depth layer (e.g., 500–5,000 m). The upper  $x$ -axis lists the methods for determining  $\tau$ , including direct measurements of inputs or processes (e.g., upwelling), models, and isotope tracer of dust and scavenging ( $^{232,230}\text{Th}$ ,  $^7\text{Be}$ ). Previously published upper ocean residence times (left and center panels) are generally  $\tau_{diss}$  (squares) and restricted to the Atlantic. This study quadruples the existing dataset, adding new export-based  $\tau_{tot}$  (stars) and  $\tau_{diss}$  (right panel). These new  $\tau$  are from diverse regions and are shorter, on average, than prior upper ocean estimates (center panel). Minimum  $\tau_{diss}$  and maximum  $\tau_{diss}$  are determined with respect to removal by biological and abiotic processes ( $F_{bio+auth}$ , Equation 5) and biological processes alone ( $F_{bio}$ , Equation 4). Reference numbers are indicated along the upper axis (1-Bergquist & Boyle, 2006; 2-Boyle et al., 2005; 3-Bruland et al., 1994; 4-Buck et al., 2010; 5-Croot et al., 2004; 6-Hayes et al., 2015; 7-Hayes, Anderson, et al., 2018; 8-Jickells, 1999; 9-Kadko et al., 2019; 10-Moore et al., 2004; 11-Sarthou et al., 2003; 12-Tagliabue et al., 2016; 13-Ussher et al., 2013).

Although most particulate, lithogenic Fe passes relatively unaltered through the upper ocean, biological and abiotic processes, such as uptake and precipitation, lead to exchange between the dissolved and particulate pools of Fe and the association of non-lithogenic Fe with sinking particles. The residence time of dissolved Fe with respect to these authigenic and biological processes (Figure 4) indicates the removal timescales of the more reactive and biologically accessible forms of Fe. Our upper ocean estimates of  $\tau_{diss}$  in this study are generally on the order of months to a few years (far right panel, Figure 3; Table 2), reflecting the wide range in inventories of dissolved Fe ( $x$ -axis, Figure 4),  $F_{bio}$  ( $y$ -axis in right panel, Figure 4), and  $F_{bio+auth}$  ( $y$ -axis in left panel, Figure 4). In the sub-Antarctic, in particular,  $\tau_{diss}$  can vary over 4 orders of magnitude from 0.5 to >5,000 days (15 years). The North Atlantic gyre and subantarctic locations with  $\tau_{diss} > 10$  years ( $n = 10$ , right panel, Figure 4) require further examination with additional radioisotope systems that can capture these timescales (e.g.,  $^{230}\text{Th}$ - $^{234}\text{U}$ ). As such, the longest  $^{234}\text{Th}$ -derived  $\tau_{diss}$  observed in these regions should be considered “apparent” residence times until further constraint is possible.

**Table 2**  
Zonal Estimates of Export and Residence Time

Parameter	Coastal	Intermediate	Gyre	High latitude North Atlantic	Sub-Antarctic-Antarctic
<b>n</b>	<b>12–26</b>	<b>18–20</b>	<b>51–61</b>	<b>9</b>	<b>15–16</b>
Mean total Fe inventory ( $\mu\text{mol m}^{-2}$ )	$781 \pm 436$	$469 \pm 415$	$115 \pm 98$	$60 \pm 35$	$213 \pm 220$
Mean dissolved Fe inventory ( $\mu\text{mol m}^{-2}$ )	$139 \pm 143$	$57 \pm 33$	$40 \pm 34$	$26 \pm 13$	$29 \pm 18$
Mean $F_{tot}$ ( $\mu\text{mol m}^{-2} \text{day}^{-1}$ )	$57 \pm 46$	$21 \pm 22$	$4 \pm 5$	$5 \pm 5$	$22 \pm 37$
Mean $F_{POC}$ ( $\mu\text{mol m}^{-2} \text{day}^{-1}$ )	$7 \pm 3$	$6 \pm 4$	$2 \pm 1$	$6 \pm 3$	$10 \pm 9$
Mean $\tau_{tot}$ (days)	$20 \pm 23$	$42 \pm 43$	$60 \pm 66$	$33 \pm 41$	$169 \pm 239$
<b>n</b>	<b>12</b>	<b>17–19</b>	<b>50–57</b>	<b>9</b>	<b>11</b>
Mean $F_{lith}$ ( $\mu\text{mol m}^{-2} \text{day}^{-1}$ )	$28 \pm 21$	$20 \pm 22$	$2 \pm 4$	$3 \pm 2$	$21 \pm 27$
Mean $F_{bio+auth}$ ( $\mu\text{mol m}^{-2} \text{day}^{-1}$ )	$26 \pm 25$	$0.6 \pm 0.7$	$1 \pm 2$	$2 \pm 3$	$10 \pm 17$
Mean $F_{bio}$ ( $\mu\text{mol m}^{-2} \text{day}^{-1}$ )	$0.8 \pm 1.3$	$0.3 \pm 0.4$	$0.1 \pm 0.1$	$0.4 \pm 0.3$	$0.1 \pm 0.1$
Mean $\tau_{lith}$ (days)	$92 \pm 223$	$35 \pm 32$	$88 \pm 96$	$28 \pm 36$	$82 \pm 168$
Median $\tau_{lith}$ (days)	21	20	47	12	15
Mean $\tau_{diss,bio+auth}$ (years)	$3 \pm 6$	$2 \pm 3$	$2 \pm 3$	$0.1 \pm 0.2$	$0.1 \pm 0.2$
Median $\tau_{diss,bio+auth}$ (years)	0.03	0.26	0.12	0.09	0.04
Mean $\tau_{diss,bio}$ (years)	$4 \pm 5$	$3 \pm 5$	$4 \pm 6$	$0.4 \pm 0.4$	$4 \pm 5$
Median $\tau_{diss,bio}$ (years)	2	1	2	0.2	1

Note. Residence times were determined at each individual location using semi-simultaneously measured Fe inventories and export fluxes at depths ranging from 40 to 225 m. Because the zonal residence times are averages of residence times for individual locations, the mean total inventory divided by the mean  $F_{tot}$  will not equal the mean residence time. Means are reported  $\pm 1$  standard deviation.  $F_{POC}$  is the export flux of particulate organic carbon. See Figure S1 for a summary schematic combining data from Figure 4 and Table 2. Note that  $\tau_{diss,bio}$  for the sub-Antarctic is likely an overestimate because seven of the 11  $F_{bio}$  were determined using a weak acid leach noted to underestimate  $F_{bio}$  (Planquette et al., 2011).

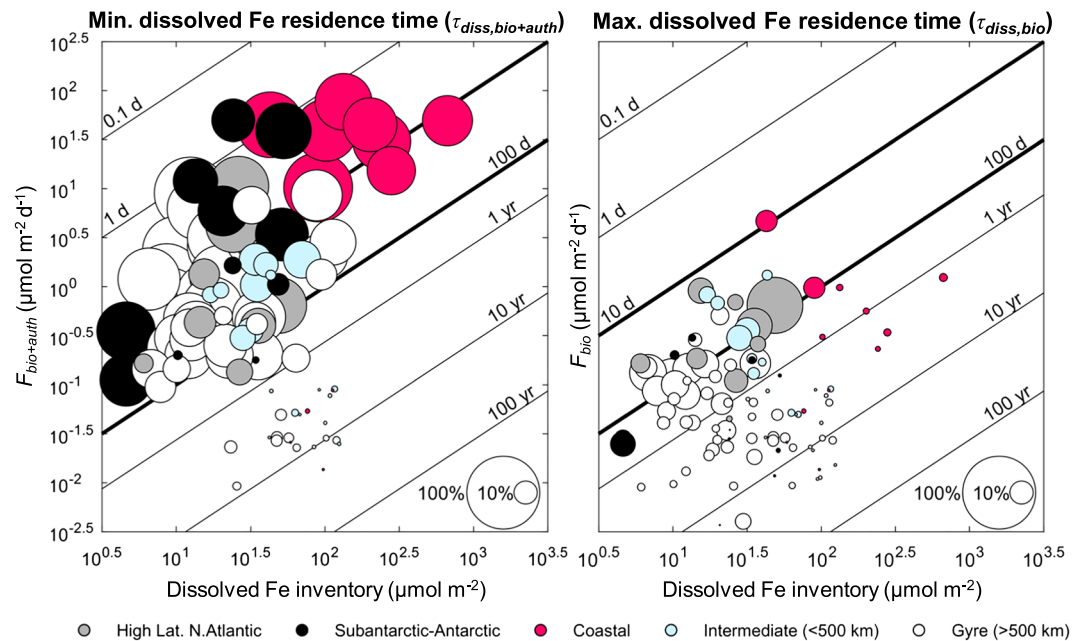


**Figure 4.** Residence times of dissolved iron. Upper ocean residence times (diagonal lines) for this study were determined using semi-simultaneously measured dissolved Fe inventories, Fe export ( $F_{tot}$ ), and element ratios from sinking particles (i.e., Fe:P and Fe:Al). The minimum (left) and maximum (right) bounds on the residence time of dissolved Fe are shown with respect to Fe removal via biological and authigenic Fe export (left,  $\tau_{bio+auth}$ ) and via biological processes only (right,  $\tau_{bio}$ ). In the left panel, the marker diameter represents  $F_{bio+auth} : F_{tot}$  or the percentage of the total Fe export that is biological Fe or authigenic Fe. In the right panel, the marker diameter is  $F_{bio} : F_{tot}$ . The data shown ( $n = 99$  for each panel) represent the locations where  $F_{bio}$  and  $F_{bio+auth}$  are calculable. Due to the sequence of determination for the flux fractions, estimates of  $F_{auth}$  are the most uncertain and in some cases are zero.

A generally longer residence time for the (potentially) more reactive fraction of the Fe pool (i.e., dissolved Fe) could seem counterintuitive, at first. However, the export of biological Fe makes up less than 5%, on average, of the total Fe flux out of the upper ocean (s.d. = 8%; circle diameter, right panel, Figure 4) and the dissolved inventory is ~30% of the total inventory. The much smaller  $F_{bio}:F_{tot}$  means that the average  $\tau_{diss,bio}$  is significantly longer than  $\tau_{tot}$  (Figure 4). The generally long  $\tau_{diss,bio}$ , relative to  $\tau_{tot}$ , indicate that the rate constant for the removal of dissolved Fe from the surface ocean via biological processes is much smaller than that for the sum of all processes removing all forms of Fe. Virtually all the  $\tau_{diss,bio}$  (95%, Table S2) fall between 20 days and 20 years, and most zonal averages (and medians) are between 1 and 4 years (Table 2).

Thirty-four percent of the paired  $F_{bio}$  and  $F_{auth}$  estimates show essentially no authigenic Fe ( $F_{bio} = F_{bio+auth}$  or  $F_{auth}:F_{tot} < 0.01$ ), and these locations are predominantly in the North Atlantic where  $F_{lith}$  dominates  $F_{tot}$ . However,  $F_{auth}$  can make up 44% of  $F_{tot}$  and is 85% of the  $F_{bio+auth}$ , on average, when present and determinable. Higher authigenic percentages are most often found at Pacific and subantarctic locations. These results and those for  $F_{lith}$  illustrate that lithogenic and authigenic Fe collectively represent the largest phases responsible for Fe export globally from the upper ocean. The abiotic cycling of lithogenic and authigenic Fe sets the particulate inventories, export fluxes, and  $\tau_{tot}$  that we observe in the surface ocean. While the biological utilization of the dissolved Fe inventory and its retention in the surface ocean is of utmost interest to ocean biogeochemists and of immediate relevance to climate modelers, it is vital to determine whether the authigenic Fe is derived from in situ abiotic processes that remove dissolved Fe, thereby affecting  $\tau_{diss}$ , or if it is formed elsewhere in the water column (e.g., at boundaries of low oxygen environments or estuaries) or external to the ocean (e.g., from weathering processes or as Fe coatings on dust) and being delivered to the sites in question.

### 3.2.1. Export-Based $\tau_{diss}$ in Context

Prior input-based studies of  $\tau_{diss}$  were conducted almost exclusively in the North-Central Atlantic Ocean (gray, Figure 3), an extremely dusty corridor whose typical surface ocean conditions likely do not represent those found in most other basins. Previous studies from other areas of the ocean found longer  $\tau_{diss}$ , on average, than the sub-annual to annual  $\tau_{diss}$  determined in this study (blue, yellow, and orange markers in Figure 3). Much of what we previously thought about  $\tau_{diss}$  from the rest of the world's oceans was based on global model estimates (e.g., 0.6–3.7 years; Moore et al., 2004), and a few observation-based estimates from the Pacific (0.5 to 17 years; Boyle et al., 2005; Hayes et al., 2015) and high latitude regions (1 to >10 years; Kadko et al., 2019; Ussher et al., 2013). Regardless of basin, most studies to date have used some measure of dust inputs or aerosol-related methods to quantify residence time (e.g., direct collection,  $^7\text{Be}$ , and  $^{232}\text{Th}$ - $^{230}\text{Th}$ ; Figure 3). Dust-based methods may inherently underestimate Fe inputs to a region that receives substantial sediment-sourced input fluxes, and so input-based residence times could appear longer than export-based estimates from the same region. Furthermore, model-based estimates of dust fluxes are thought to underestimate true dust inputs in some regions of the global ocean (e.g., the Equatorial Pacific; Winckler et al., 2008), which would also create longer apparent residence times for Fe. Nevertheless, this does not seem a likely explanation for the comparatively longer, measurement-based residence times previously determined for the central Pacific and other factors likely play a more important role in the apparent offset in  $\tau_{diss}$ . Unfortunately, the limited number of historical data points prevents a more rigorous, global method comparison outside of the North Atlantic.

Ideally, dust and export measurements used for residence time estimates would capture conditions or events that are representative of a part of the ocean for a given timescale of interest (e.g., seasonally or annually). However, a local productivity bloom could lead to rapid export of Fe, and a storm-related dust delivery could introduce a substantial amount of new Fe to the upper ocean in a single day. If a study captures a high input or output event and the location is never revisited, the residence time determined for this region might not represent average conditions over annual timescales, for example. Now with an abundance of multi-method data for the North Atlantic, the existing range in regional and temporal conditions is clearly visible and the  $\tau_{diss}$  found in this study overlap quite well with previous  $\tau_{diss}$  estimates from the Atlantic (gray, Figure 3). With only the prior data outside of the North Atlantic, we could not assess this natural variability, and perhaps, some of the longer historical estimates of  $\tau_{diss}$  simply captured atypical conditions for their region. Conversely, in the Arctic Ocean, the authors of a  $^7\text{Be}$  atmospheric input-based study attributed their abnormally long  $\tau_{diss}$  (yellow, center panel, Figure 3) to additional inputs from the transpolar drift (Kadko

et al., 2019). These  $\tau_{diss}$  could very well be the typical conditions for the central Arctic, but until an alternate method is utilized in this region, we cannot know how normal or atypical these longer  $\tau_{diss}$  may be in the Arctic or elsewhere. The overlap between prior and new  $\tau_{diss}$  from the North Atlantic is encouraging, especially with the diversity of methods employed; however, far too many data gaps still exist (e.g., in the Indian Ocean, North Pacific, and the Arctic Ocean; Figure 1), and this data compilation shows that a single time point estimate covering thousands of kilometers of ocean could considerably misrepresent the typical conditions of a given region.

#### 4. Conclusions: Insights Gained and Future Directions

GEOTRACES-based synthesis efforts like this one help to close the gap between our observational- and model-based understanding of global Fe cycling by bringing together prior and new results with which to test and improve ocean models. A robust finding from our synthesis covering a wide range of Fe sources and biogeographical provinces is that the export flux of particulate Fe from the upper ocean scales with the inventory of Fe above the depth of export. Consequently,  $\tau_{tot}$  is relatively invariant among these regions (67% of results fall between 10 and 100 days) despite a range of Fe inventories that span more than two orders of magnitude. Furthermore, the rate constant for export of total Fe ( $\lambda_{tot}$ ), the inverse of  $\tau_{tot}$  and a parameter to be coded into ocean biogeochemical models, is now well constrained (0.01–1 day<sup>-1</sup>) for much of the global ocean, the exception being the sub-Antarctic. The time scale for the export of total Fe is similar to that for the export of total particulate matter, and thus, future investigation of the factors regulating  $\lambda$  for particle aggregation and sinking through the upper water column, for example, using multiple Th isotopes (e.g., <sup>234</sup>Th-<sup>238</sup>U, <sup>228</sup>Th-<sup>228</sup>Ra, and <sup>230</sup>Th-<sup>234</sup>U) (Hayes, Black, et al., 2018), will lead to both more precise and mechanistic constraints on the conditions that regulate Fe cycling in the upper ocean.

Within the global data set studied here, the residence time of dissolved Fe ( $\tau_{diss}$ ) exhibits a greater range of variability than for total Fe. One factor contributing to this variability may be the assumption of steady state used to derive  $\tau_{diss}$  from measured inventories and export fluxes. Time series studies long enough to sample across natural variability of dissolved Fe supply and removal processes will be necessary to define non-steady state conditions that may contribute to the apparent variability of  $\tau_{diss}$ . Variability of local environmental conditions, such as the dissolved Fe to nitrate ratio, may also contribute to the apparent variability of  $\tau_{diss}$ . For example, recent studies indicate that marine microbes can upregulate genes to produce ligands with stronger Fe-binding constants when other conditions, such as an abundance of macronutrients (e.g., nitrate), favor Fe retention and recycling within the euphotic zone (Boiteau et al., 2016, 2019). Future process studies that combine radionuclide-based estimates of  $\tau_{diss}$ , like those employed here, measurements of ligand composition and binding constants, and the tools of molecular biology (e.g., proteomics) that indicate the response of organisms to their chemical environment, will help define the conditions under which marine ecosystems expend the additional energy needed to retain and recycle Fe (Rafter et al., 2017). These conditions are currently poorly constrained in global biogeochemical models.

Lastly, we note that the uncertainties in  $\tau_{diss}$  can be reduced through additional investigation of two assumptions inherent in its derivation. First, the biogenic Fe content of particles used in our calculations is based on measured cell quotas of Fe and P for a relatively small number of samples. Expanding the database of these quotas to better establish their natural range and patterns of variability, and matching estimates of particulate biogenic Fe concentration to cell quotas determined concurrently with the biogenic Fe estimates, will reduce the uncertainty in the derived biogenic Fe fluxes. Second, the inability to determine whether in situ authigenic Fe originated locally (e.g., precipitation) or was transported (e.g., as Fe oxide coatings on dust) imposes a large uncertainty in the actual time scale that dissolved Fe remains within the biologically active upper ocean. Since authigenic Fe may constitute several tens of percent of the total particulate Fe in some cases, identifying the source and bioavailability of particulate authigenic Fe would be a high priority for future studies. Planning for studies such as those identified here can begin now, during the final years of the global survey of the distribution of Fe and other trace elements in the ocean by the international GEOTRACES program.

#### Conflict of Interest

The authors have no conflicts of interest.



## Data Availability Statement

All original U.S. GEOTRACES data are available through the Biological and Chemical Oceanography Data Management Office (BCO-DMO) and derived data compilations of new and prior datasets have been made available in the supporting information. The BCO-DMO websites listed below include all the metadata and relevant links. To reach the data page for each, either scroll down to the “Data URL” link on the main page or simply add “/data” to the BCO-DMO http listed below (e.g., <http://lod.bco-dmo.org/id/dataset/3662/data>). The following were used to determine new iron export and residence times for TN303, KN199-04, and KN204-01:

Boyle, E. (2013), Bottle data along with US GEOTRACES North Atlantic Transect from the R/V Knorr KN204-01 cruise in the subtropical N. Atlantic during 2011 (U.S. GEOTRACES NAT project). Biological and Chemical Oceanography Data Management Office (BCO-DMO). Dataset version 2013-02-13. <http://lod.bco-dmo.org/id/dataset/3662> [last access: 2018-06-12].

Buesseler, K., Charette, M. and Moore, W. (2018), Particulate Th-234 from in-situ pumps, including large size fraction (>51  $\mu\text{m}$ ) and small size fraction (1–51  $\mu\text{m}$ ), from R/V Thomas G. Thompson cruise TN303 in the Eastern Tropical Pacific in 2013 (U.S. GEOTRACES EPZT project). Biological and Chemical Oceanography Data Management Office (BCO-DMO). Dataset version: 2018-04-20. <http://lod.bco-dmo.org/id/dataset/643316> [last access: 2018-06-04].

Buesseler, K., Charette, M., & Moore, W. (2017), Water-column total Th-234 and U-238 from R/V Thomas G. Thompson cruise TN303 in the Eastern Tropical Pacific in 2013 (U.S. GEOTRACES EPZT project). Biological and Chemical Oceanography Data Management Office (BCO-DMO). Dataset version: 2017-01-27. <http://www.bco-dmo.org/dataset/643213> [last access: 2018-06-04].

Buesseler, K. (2013), Particulate Thorium-234 from in situ pumps from R/V Knorr cruises KN199-04 and KN204-01 in the Subtropical northern Atlantic Ocean from 2010–2011 (U.S. GEOTRACES NAT project). Biological and Chemical Oceanography Data Management Office (BCO-DMO). Dataset version: 2013-03-06. <http://lod.bco-dmo.org/id/dataset/3835> [last access: 2018-06-04].

Buesseler, K. (2013), Water-column total Thorium-234 and Uranium-238 from R/V Knorr cruises KN199-04 and KN204-01 in the Subtropical northern Atlantic Ocean from 2010–2011 (U.S. GEOTRACES NAT project). Biological and Chemical Oceanography Data Management Office (BCO-DMO). Dataset version: 2013-03-05. <http://lod.bco-dmo.org/id/dataset/3836> [last access: 2018-06-04].

John, S. (2016), Dissolved Fe, Zn and Cd concentrations and isotope ratios from R/V Knorr KN199-04, KN204-01 in the subtropical North Atlantic Ocean from 2010–2011 (U.S. GEOTRACES NAT project). Biological and Chemical Oceanography Data Management Office (BCO-DMO). Dataset version 2016-11-30. <http://lod.bco-dmo.org/id/dataset/3840> [last access: 2018-06-04].

Lam, P. (2017), Size-fractionated major and minor particle composition and concentration collected from RV Thompson (TN303) along the US GEOTRACES EPZT transect in the Eastern Tropical Pacific during 2013 (US GEOTRACES EPZT project). Biological and Chemical Oceanography Data Management Office (BCO-DMO). Dataset version: 2017-01-03. <http://lod.bco-dmo.org/id/dataset/668083> [last access: 2018-06-04].

Lam, P. (2014), Size-fractionated major and minor particle composition and concentration from R/V Knorr KN199-04, KN204-01 in the subtropical North Atlantic Ocean from 2010–2011 (U.S. GEOTRACES NAT project). Biological and Chemical Oceanography Data Management Office (BCO-DMO). Dataset version: 2014-12-12. <http://lod.bco-dmo.org/id/dataset/3871> [last access: 2018-06-04].

Sedwick, P. and Resing, J. (2016), Water-column dissolved iron (Fe) concentrations for major stations occupied during U.S. GEOTRACES EPZT cruise (R/V Thomas G. Thompson TN303) from October to December 2013; post-cruise analyses conducted at Old Dominion University. Biological and Chemical Oceanography Data Management Office (BCO-DMO). Dataset version 2016-12-19. <http://lod.bco-dmo.org/id/dataset/670285> [last access: 2018-06-04].

In addition to published dissolved and particulate Fe data, from Tonnard et al. (2020) and Gourain et al. (2019) respectively, the following was used to determine new iron export and residence times for GEOVIDE:

Lemaitre, N. (2017), Multi-proxy approach (234Th, Baxs) of export and remineralization fluxes of carbon and biogenic elements associated with the oceanic biological pump. Universite de Bretagne Occidentale. NNT: 2017BRES0009. Tel-01578408. <https://tel.archives-ouvertes.fr/tel-01578408/document> [last access: 2020-02-27].

The following were used to determine chlorophyll-a, net primary production, and ocean current speeds: Earth Space Research, ESR (2009), OSCAR third degree resolution ocean surface currents. Ver. 1. PO. DAAC, CA, USA. <https://doi.org/10.5067/OSCAR-03D01>. [last access: 2018-06-19].

NASA Goddard Space Flight Center, Ocean Biology Processing Group (2018), Moderate-resolution imaging spectroradiometer (MODIS) Ocean Color Data, NASA OB.DAAC, Greenbelt, MD, USA. <https://ocean-data.sci.gsfc.nasa.gov/MODIS-Aqua/Mapped/Annual/> [last access: 2018-06-22].

NOAA (2013), World Ocean Atlas statistical mean of percent oxygen saturation on 1° grid for all decades. Dataset version WOA2013. <https://www.nodc.noaa.gov/cgi-bin/OC5/woa13/woa13oxnu.pl?parameter=O>. [last access: 2018-06-19].

Ocean Productivity, Oregon State University, (2018), Custom products: updated Cup, <http://www.science.oregonstate.edu/ocean.productivity/custom.php> [last access: 20 Jun 2018].

### Acknowledgments

We would like to thank S. Albani for providing the dust model results (Community Atmosphere Model, C4fn) and the three anonymous reviewers for their constructive comments. The U.S. GEOTRACES work was supported by the National Science Foundation (OCE-1232669 and OCE-1518110) and E. Black was also funded by a NASA Earth and Space Science Graduate Fellowship (NNX13AP31H) and the Ocean Frontier Institute. The GEOVIDE work was funded by the Flanders Research Foundation (G071512N), the Vrije Universiteit Brussel (SRP-2), the French ANR Blanc GEOVIDE (ANR-13-BS06-0014), ANR RPDOC BITMAP (ANR-12-PDOC-0025-01), IFREMER, CNRS-INSU (programme LEFE), INSU OPTIMISP, and Labex-Mer (ANR-10-LABX-19).

### References

- Albani, S., Mahowald, N. M., Perry, A. T., Scanza, R. A., Zender, C. S., Heavens, N. G., et al. (2014). Improved dust representation in the Community Atmosphere Model. *Journal of Advances in Modeling Earth Systems*, *6*, 541–570. <https://doi.org/10.1002/2013MS000279>. Received
- Ardayna, M., Lacour, L., Sergi, S., d'Ovidio, F., Sallée, J. B., Rembauville, M., et al. (2019). Hydrothermal vents trigger massive phytoplankton blooms in the Southern Ocean. *Nature Communications*, *10*(1), 2451–2458. <https://doi.org/10.1038/s41467-019-09973-6>
- Barrett, P. M., Resing, J. A., Grand, M. M., Measures, C. I., & Landing, W. M. (2018). Trace element composition of suspended particulate matter along three meridional CLIVAR sections in the Indian and Southern Oceans: Impact of scavenging on Al distributions. *Chemical Geology*, *502*, 15–28. <https://doi.org/10.1016/j.chemgeo.2018.06.015>
- Bergquist, B. A., & Boyle, E. A. (2006). Dissolved iron in the tropical and subtropical Atlantic Ocean. *Global Biogeochemical Cycles*, *20*, GB1015. <https://doi.org/10.1029/2005GB002505>
- Bishop, J. K., Edmond, J. M., Ketten, D. R., Bacon, M. P., & Silker, W. B. (1977). The chemistry, biology, and vertical flux of particulate matter from the upper 400 m of the equatorial Atlantic Ocean. *Deep-Sea Research*, *24*, 511–548.
- Black, E. E., Buesseler, K. O., Pike, S. M., & Lam, P. J. (2018). <sup>234</sup>Th as a tracer of particulate export and remineralization in the southeastern tropical Pacific. *Marine Chemistry*, *201*, 35–50. <https://doi.org/10.1016/j.marchem.2017.06.009>
- Black, E. E., Lam, P. J., Lee, J.-M., & Buesseler, K. O. (2019). Insights from the <sup>238</sup>U-<sup>234</sup>Th method into the coupling of biological export and the cycling of cadmium, cobalt, and manganese in the Southeast Pacific Ocean. *Global Biogeochemical Cycles*, *33*, 15–36. <https://doi.org/10.1029/2018GB005985>
- Boiteau, R. M., Mende, D. R., Hawco, N. J., McIlvin, M. R., Fitzsimmons, J. N., Saito, M. A., et al. (2016). Siderophore-based microbial adaptations to iron scarcity across the eastern Pacific Ocean. *Proceedings of the National Academy of Sciences*, *113*(50), 14,237–14,242. <https://doi.org/10.1073/pnas.1608594113>
- Boiteau, R. M., Till, C. P., Coale, T. H., Fitzsimmons, J. N., Bruland, K. W., & Repeta, D. J. (2019). Patterns of iron and siderophore distributions across the California current system. *Limnology and Oceanography*, *64*(1), 376–389. <https://doi.org/10.1002/lno.11046>
- Bowie, A. R., Lannuzel, D., Remenyi, T. A., Wagener, T., Lam, P. J., Boyd, P. W., et al. (2009). Biogeochemical iron budgets of the Southern Ocean south of Australia: Decoupling of iron and nutrient cycles in the subantarctic zone by the summertime supply. *Global Biogeochemical Cycles*, *23*, GB4034. <https://doi.org/10.1029/2009GB003500>
- Bowie, A. R., van der Merwe, P., Quéroué, F., Trull, T., Fourquez, M., Planchon, F., et al. (2015). Iron budgets for three distinct biogeochemical sites around the Kerguelen Archipelago (Southern Ocean) during the natural fertilisation study, KEOPS-2. *Biogeosciences*, *12*(14), 4421–4445. <https://doi.org/10.5194/bg-12-4421-2015>
- Boyd, P. W., Mackie, D. S., & Hunter, K. A. (2010). Aerosol iron deposition to the surface ocean—Modes of iron supply and biological responses. *Marine Chemistry*, *120*(1–4), 128–143. <https://doi.org/10.1016/j.marchem.2009.01.008>
- Boyle, E. A., Bergquist, B. A., Kayser, R. A., & Mahowald, N. (2005). Iron, manganese, and lead at Hawaii Ocean Time-series station ALOHA: Temporal variability and an intermediate water hydrothermal plume. *Geochimica et Cosmochimica Acta*, *69*(4), 933–952. <https://doi.org/10.1016/j.gca.2004.07.034>
- Bruland, K. W., Orians, K. J., & Cowen, J. P. (1994). Reactive trace metals in the stratified central North Pacific. *Geochimica et Cosmochimica Acta*, *58*(15), 3171–3182. [https://doi.org/10.1016/0016-7037\(94\)90044-2](https://doi.org/10.1016/0016-7037(94)90044-2)
- Bruland, K. W., Rue, E. L., Smith, G. J., & DiTullio, G. R. (2005). Iron, macronutrients and diatom blooms in the Peru upwelling regime: Brown and blue waters of Peru. *Marine Chemistry*, *93*(2–4), 81–103. <https://doi.org/10.1016/j.marchem.2004.06.011>
- Buck, C. S., Aguilar-Islas, A., Marsay, C., Kadko, D., & Landing, W. M. (2019). Trace element concentrations, elemental ratios, and enrichment factors observed in aerosol samples collected during the US GEOTRACES eastern Pacific Ocean transect (GP16). *Chemical Geology*, *511*, 212–224. <https://doi.org/10.1016/j.chemgeo.2019.01.002>
- Buck, C. S., Landing, W. M., Resing, J. A., & Measures, C. I. (2010). The solubility and deposition of aerosol Fe and other trace elements in the North Atlantic Ocean: Observations from the A16N CLIVAR/CO<sub>2</sub> repeat hydrography section. *Marine Chemistry*, *120*(1–4), 57–70. <https://doi.org/10.1016/j.marchem.2008.08.003>
- Collier, R., Dymond, J., Honjo, S., Manganini, S., Francois, R., & Dunbar, R. (2000). The vertical flux of biogenic and lithogenic material in the Ross Sea: Moored sediment trap observations 1996–1998. *Deep Sea Research, Part II*, *47*(15–16), 3491–3520. [https://doi.org/10.1016/S0967-0645\(00\)00076-X](https://doi.org/10.1016/S0967-0645(00)00076-X)
- Croot, P. L., Frew, R. D., Sander, S., Hunter, K. A., Ellwood, M. J., Pickmere, S. E., et al. (2007). Physical mixing effects on iron biogeochemical cycling: FeCycle experiment. *Journal of Geophysical Research*, *112*, C06015. <https://doi.org/10.1029/2006JC003748>
- Croot, P. L., Streu, P., & Baker, A. R. (2004). Short residence time for iron in surface seawater impacted by atmospheric dry deposition from Saharan dust events. *Geophysical Research Letters*, *31*, L23S08. <https://doi.org/10.1029/2004GL020153>
- Cutter, G. A., & Bruland, K. W. (2012). Rapid and noncontaminating sampling system for trace elements in global ocean surveys. *Limnology and Oceanography: Methods*, *10*, 425–436. <https://doi.org/10.4319/lom.2012.10.425>
- Ducklow, H. H. W., Steinberg, D. D. K., Buessler, K., & Buesseler, K. O. (2001). Upper ocean carbon export and the biological pump. *Oceanography*, *14*(4), 50–58. <https://doi.org/10.5670/oceanog.2001.06>

- Ellwood, M. J., Nodder, S. D., King, A. L., Hutchins, D. A., Wilhelm, S. W., & Boyd, P. W. (2014). Pelagic iron cycling during the subtropical spring bloom, east of New Zealand. *Marine Chemistry*, *160*, 18–33. <https://doi.org/10.1016/j.marchem.2014.01.004>
- Frew, R. D., Hutchins, D. A., Nodder, S., Sanudo-Wilhelmy, S., Tovar-Sanchez, A., Leblanc, K., et al. (2006). Particulate iron dynamics during FeCycle in subantarctic waters southeast of New Zealand. *Global Biogeochemical Cycles*, *20*, GB1S93. <https://doi.org/10.1029/2005GB002558>
- Gautier, I., Weis, D., Mennessier, J. P., Vidal, P., Giret, A., & Loubet, M. (1990). Petrology and geochemistry of the Kerguelen Archipelago basalts (South Indian Ocean): Evolution of the mantle sources from ridge to intraplate position. *Earth and Planetary Science Letters*, *100*(1–3), 59–76. [https://doi.org/10.1016/0012-821X\(90\)90176-X](https://doi.org/10.1016/0012-821X(90)90176-X)
- Gehlen, M., Beck, L., Calas, G., Flank, A. M., van Bennekom, A. J., & van Beusekom, J. E. E. (2002). Unraveling the atomic structure of biogenic silica: Evidence of the structural association of Al and Si in diatom frustules. *Geochimica et Cosmochimica Acta*, *66*(9), 1601–1609. [https://doi.org/10.1016/S0016-7037\(01\)00877-8](https://doi.org/10.1016/S0016-7037(01)00877-8)
- Gourain, A., Planquette, H., Cheize, M., Lemaitre, N., Menzel Barraqueta, J. L., Shelley, R., et al. (2019). Inputs and processes affecting the distribution of particulate iron in the North Atlantic along the GEOVIDE (GEOTRACES GA01) section. *Biogeosciences*, *16*(7), 1563–1582. <https://doi.org/10.5194/bg-16-1563-2019>
- Gunn, B. M., Coy-Yll, R., Watkins, N. D., Abranson, C. E., & Nougier, J. (1970). Geochemistry of an oceanite-ankaramite-basalt suite from East Island, Crozet Archipelago. *Contributions to Mineralogy and Petrology*, *28*(4), 319–339. <https://doi.org/10.1007/BF00388954>
- Hayes, C. T., Black, E. E., Anderson, R. F., Baskaran, M., Buesseler, K. O., Charette, M. A., et al. (2018). Flux of particulate elements in the North Atlantic Ocean constrained by multiple radionuclides. *Global Biogeochemical Cycles*, *32*, 1738–1758. <https://doi.org/10.1029/2018GB005994>
- Hayes, C. T., Anderson, R. F., Cheng, H., Conway, T. M., Edwards, R. L., Fleisher, M. Q., et al. (2018). Replacement times of a spectrum of elements in the North Atlantic based on thorium supply. *Global Biogeochemical Cycles*, *32*, 1294–1311. <https://doi.org/10.1029/2017GB005839>
- Hayes, C. T., Fitzsimmons, J. N., Boyle, E. A., Mcgee, D., Anderson, R. F., Weisend, R., & Morton, P. L. (2015). Thorium isotopes tracing the iron cycle at the Hawaii Ocean Time-series Station ALOHA. *Geochimica et Cosmochimica Acta*, *169*, 1–16. <https://doi.org/10.1016/j.gca.2015.07.019>
- Holmes, T. M., Chase, Z., van der Merwe, P., Townsend, A. T., & Bowie, A. R. (2017). Detection, dispersal and biogeochemical contribution of hydrothermal iron in the ocean. *Marine and Freshwater Research*, *68*(12), 2184–2204. <https://doi.org/10.1071/MF16335>
- Jickells, T. D. (1999). The inputs of dust derived elements to the Sargasso Sea: a synthesis. *Marine Chemistry*, *68*(1–2), 5–14. [https://doi.org/10.1016/S0304-4203\(99\)00061-4](https://doi.org/10.1016/S0304-4203(99)00061-4)
- Kadko, D., Aguilar-Islas, A., Bolt, C., Buck, C. S., Fitzsimmons, J. N., Jensen, L. T., et al. (2019). The residence times of trace elements determined in the surface Arctic Ocean during the 2015 US Arctic GEOTRACES expedition. *Marine Chemistry*, *208*, 56–69. <https://doi.org/10.1016/j.marchem.2018.10.011>
- Knox, F., & McElroy, M. B. (1984). Changes in atmospheric CO<sub>2</sub>: Influence of the marine biota at high latitude. *Journal of Geophysical Research*, *89*(D3), 4629–4637. <https://doi.org/10.1029/JD089iD03p04629>
- Kudela, R. M., Garfield, N., & Bruland, K. W. (2006). Bio-optical signatures and biogeochemistry from intense upwelling and relaxation in coastal California. *Deep-Sea Research Part II: Topical Studies in Oceanography*, *53*(25–26), 2999–3022. <https://doi.org/10.1016/j.dsr2.2006.07.010>
- Lam, P. J., Lee, J. M., Heller, M. I., Mehic, S., Xiang, Y., & Bates, N. R. (2018). Size-fractionated distributions of suspended particle concentration and major phase composition from the U.S. GEOTRACES Eastern Pacific Zonal Transect (GP16). *Marine Chemistry*, *201*, 90–107. <https://doi.org/10.1016/j.marchem.2017.08.013>
- Lamborg, C. H., Buesseler, K. O., & Lam, P. J. (2008). Sinking fluxes of minor and trace elements in the North Pacific Ocean measured during the VERTIGO program. *Deep-Sea Research Part II: Topical Studies in Oceanography*, *55*(14–15), 1564–1577. <https://doi.org/10.1016/j.dsr2.2008.04.012>
- Landing, W. M., & Bruland, K. W. (1987). The contrasting biogeochemistry of manganese and iron in the Pacific Ocean. *Geochimica et Cosmochimica Acta*, *51*, 29–43. [https://doi.org/10.1016/0016-7037\(87\)90004-4](https://doi.org/10.1016/0016-7037(87)90004-4)
- Lannuzel, D., Bowie, A. R., Remenyi, T., Lam, P., Townsend, A., Ibsanmi, E., et al. (2011). Distributions of dissolved and particulate iron in the sub-Antarctic and Polar Frontal Southern Ocean (Australian sector). *Deep-Sea Research Part II: Topical Studies in Oceanography*, *58*(21–22), 2094–2112. <https://doi.org/10.1016/j.dsr2.2011.05.027>
- Lemaitre, N., Planchon, F., Planquette, H., Dehairs, F., Fonseca-Batista, D., Roukaerts, A., et al. (2018). High variability of export fluxes along the North Atlantic GEOTRACES section GA01: Particulate organic carbon export deduced from the <sup>234</sup>Th method. *Biogeosciences Discussions*, 1–38. <https://doi.org/10.5194/bg-2018-190>
- Lemaitre, N., Planquette, H., Dehairs, F., van der Merwe, P., Bowie, A. R., Trull, T. W., et al. (2016). Impact of the natural Fe-fertilization on the magnitude, stoichiometry and efficiency of particulate biogenic silica, nitrogen and iron export fluxes. *Deep Sea Research, Part I*, *117*(11–27). <https://doi.org/10.1016/j.dsr.2016.09.002>
- Longhurst, A. (2007). *Ecological geography of the sea* (2nd ed.). Burlington, MA: Academic Press. <https://doi.org/10.1016/B978-012455521-1/50002-4>
- Martin, J. H. (1990). Glacial-interglacial CO<sub>2</sub> change: The iron hypothesis. *Paleoceanography*, *5*(1), 1–13. <https://doi.org/10.1029/PA005i001p00001>
- Martin, J. H., Coale, K. H., Johnson, K. S., Fitzwater, S. E., Gordon, R. M., Tanner, S. J., et al. (1994). Testing the iron hypothesis in ecosystems of the equatorial Pacific Ocean. *Nature*, *371*(6493), 123–129. <https://doi.org/10.1038/371123a0>
- Martínez-García, A., Sigman, D. M., Ren, H., Anderson, R. F., Straub, M., Hodell, D. A., et al. (2014). Iron fertilization of the Subantarctic Ocean during the last ice age. *Science*, *343*(6177), 1347–1350. <https://doi.org/10.1126/science.1246848>
- McDonnell, A. M. P., & Buesseler, K. O. (2010). Variability in the average sinking velocity of marine particles. *Limnology and Oceanography*, *55*(5), 2085–2096. <https://doi.org/10.4319/lo.2010.55.5.2085>
- McLennan, S. M. (2001). Relationships between the trace element composition of sedimentary rocks and upper continental crust. *Geochemistry, Geophysics, Geosystems*, *2*(4). <https://doi.org/10.1029/2000GC000109>
- Measures, C. I., & Vink, S. (2001). Dissolved Fe in the upper waters of the Pacific sector of the Southern Ocean. *Deep Sea Research, Part II*, *48*, 3913–3941.
- Middag, R., van Hulten, M. M. P., van Aken, H. M., Rijkenberg, M. J. A., Gerringa, L. J. A., Laan, P., & de Baar, H. J. W. (2015). Dissolved aluminium in the ocean conveyor of the West Atlantic Ocean: Effects of the biological cycle, scavenging, sediment resuspension and hydrography. *Marine Chemistry*, *177*, 69–86. <https://doi.org/10.1016/j.marchem.2015.02.015>

- Moore, C. M., Mills, M. M., Arrigo, K. R., Berman-Frank, I., Bopp, L., Boyd, P. W., et al. (2013). Processes and patterns of oceanic nutrient limitation. *Nature Geoscience*, *6*(9), 701–710. <https://doi.org/10.1038/ngeo1765>
- Moore, J. K., Doney, S. C., & Lindsay, K. (2004). Upper ocean ecosystem dynamics and iron cycling in a global three-dimensional model. *Global Biogeochemical Cycles*, *18*, GB4028. <https://doi.org/10.1029/2004GB002220>
- Noble, A. E., Lamborg, C. H., Ohnemus, D. C., Lam, P. J., Goepfert, T. J., Measures, C. I., et al. (2012). Basin-scale inputs of cobalt, iron, and manganese from the Benguela-Angola front to the South Atlantic Ocean. *Limnology and Oceanography*, *57*(4), 989–1010. <https://doi.org/10.4319/lo.2012.57.4.0989>
- Ohnemus, D. C., Rauschenberg, S., Cutter, G. A., Fitzsimmons, J. N., Sherrell, R. M., & Twining, B. S. (2016). Elevated trace metal content of prokaryotic plankton communities associated with marine oxygen deficient zones. *Limnology and Oceanography*, *62*(1), 3–25. <https://doi.org/10.1002/lno.10363>
- Owens, S. A., Buesseler, K. O., & Sims, K. W. W. (2011). Re-evaluating the  $^{238}\text{U}$ -salinity relationship in seawater: Implications for the  $^{238}\text{U}$ - $^{234}\text{Th}$  disequilibrium method. *Marine Chemistry*, *127*, 31–39. <https://doi.org/10.1016/j.marchem.2011.07.005>
- Owens, S. A., Pike, S., & Buesseler, K. O. (2015). Thorium-234 as a tracer of particle dynamics and upper ocean export in the Atlantic Ocean. *Deep Sea Research, Part II*, *116*, 42–59. <https://doi.org/10.1016/j.dsr2.2014.11.010>
- Pike, S. M., Buesseler, K. O., Andrews, J., & Savoye, N. (2005). Quantification of  $^{234}\text{Th}$  recovery in small volume sea water samples by inductively coupled plasma mass spectrometry. *Journal of Radioanalytical and Nuclear Chemistry*, *263*(2), 355–360.
- Planquette, H., Sanders, R. R., Statham, P. J., Morris, P. J., & Fones, G. R. (2011). Fluxes of particulate iron from the upper ocean around the Crozet Islands: A naturally iron-fertilized environment in the Southern Ocean. *Global Biogeochemical Cycles*, *25*, GB2011. <https://doi.org/10.1029/2010GB003789>
- Planquette, H., Statham, P. J., Fones, G. R., Charette, M. A., Moore, C. M., Salter, I., et al. (2007). Dissolved iron in the vicinity of the Crozet Islands, Southern Ocean. *Deep-Sea Research Part II: Topical Studies in Oceanography*, *54*(18–20), 1999–2019. <https://doi.org/10.1016/j.dsr2.2007.06.019>
- Pohl, C., Löffler, A., & Hennings, U. (2004). A sediment trap flux study for trace metals under seasonal aspects in the stratified Baltic Sea (Gotland Basin;  $57^{\circ}19.20'\text{N}$ ;  $20^{\circ}03.00'\text{E}$ ). *Marine Chemistry*, *84*(3–4), 143–160. <https://doi.org/10.1016/j.marchem.2003.07.002>
- Primeau, F. (2005). Characterizing transport between the surface mixed layer and the ocean interior with a forward and adjoint global ocean transport model. *Journal of Physical Oceanography*, *35*(4), 545–564. <https://doi.org/10.1175/JPO2699.1>
- Quéroué, F., Sarthou, G., Planquette, H. F., Bucciarelli, E., Chever, F., van der Merwe, P., et al. (2015). High variability in dissolved iron concentrations in the vicinity of the Kerguelen Islands (Southern Ocean). *Biogeosciences*, *12*(12), 3869–3883. <https://doi.org/10.5194/bg-12-3869-2015>
- Quetel, C. R., Remoudaki, E., Davies, J. E., Miquel, J. C., Fowler, S. W., Lambert, C. E., et al. (1993). Impact of atmospheric deposition on particulate iron flux and distribution in northwestern Mediterranean waters. *Deep Sea Research, Part I*, *40*(5), 989–1002. [https://doi.org/10.1016/0967-0637\(93\)90085-H](https://doi.org/10.1016/0967-0637(93)90085-H)
- Rafter, P. A., Sigman, D. M., & Mackey, K. R. M. (2017). Recycled iron fuels new production in the eastern equatorial Pacific Ocean. *Nature Communications*, *8*(1), 1100. <https://doi.org/10.1038/s41467-017-01219-7>
- Rudnick, R. L., & Gao, S. (2014). Chapter 4.1 Composition of the continental crust. In *Treatise on geochemistry* (2nd ed., Vol. 4, pp. 1–51). New York: Elsevier Ltd. <https://doi.org/10.1016/B978-0-08-095975-7.00301-6>
- Sañial, V., Kipp, L. E., Henderson, P. B., van Beek, P., Reyss, J. L., Hammond, D. E., et al. (2018). Radium-228 as a tracer of dissolved trace element inputs from the Peruvian continental margin. *Marine Chemistry*, *201*(20–34), 20–34. <https://doi.org/10.1016/j.marchem.2017.05.008>
- Sarthou, G., Baker, A. R., Blain, S., Achterberg, E. P., Boye, M., Bowie, A. R., et al. (2003). Atmospheric iron deposition and sea-surface dissolved iron concentrations in the eastern Atlantic Ocean. *Deep-Sea Research Part I: Oceanographic Research Papers*, *50*(10–11), 1339–1352. [https://doi.org/10.1016/S0967-0637\(03\)00126-2](https://doi.org/10.1016/S0967-0637(03)00126-2)
- Schübler, U., Schulz-Bull, D. E., & Bauerfeind, E. (1997). Annual fluxes of particulate chemical trace compounds during the North-East water polynya experiment. *Journal of Marine Systems*, *10*(1–4), 391–400. [https://doi.org/10.1016/S0924-7963\(96\)00077-2](https://doi.org/10.1016/S0924-7963(96)00077-2)
- Shelley, R. U., Morton, P. L., & Landing, W. M. (2015). Elemental ratios and enrichment factors in aerosols from the US-GEOTRACES North Atlantic transects. *Deep-Sea Research Part II: Topical Studies in Oceanography*, *116*, 262–272. <https://doi.org/10.1016/j.dsr2.2014.12.005>
- Sholkovitz, E. R., Sedwick, P. N., Church, T. M., Baker, A. R., & Powell, C. F. (2012). Fractional solubility of aerosol iron: Synthesis of a global-scale data set. *Geochimica et Cosmochimica Acta*, *89*, 173–189. <https://doi.org/10.1016/j.gca.2012.04.022>
- Smith, J. N., Yeats, P. A., Knowlton, S. E., & Moran, S. B. (2014). Comparison of  $^{234}\text{Th}$ / $^{238}\text{U}$  and mass balance models for estimating metal removal fluxes in the Gulf of Maine and Scotian Shelf. *Continental Shelf Research*, *77*, 107–117. <https://doi.org/10.1016/j.csr.2014.01.008>
- Stanley, R. H. R., Buesseler, K. O., Manganini, S. J., Steinberg, D. K., & Valdes, J. R. (2004). A comparison of major and minor elemental fluxes collected in neutrally buoyant and surface-tethered sediment traps. *Deep Sea Research, Part I*, *51*(10), 1387–1395. <https://doi.org/10.1016/j.dsr.2004.05.010>
- Tagliabue, A., Bowie, A. R., DeVries, T., Ellwood, M. J., Landing, W. M., Milne, A., et al. (2019). The interplay between regeneration and scavenging fluxes drives ocean iron cycling. *Nature Communications*, *10*(1), 4960–4968. <https://doi.org/10.1038/s41467-019-12775-5>
- Tagliabue, A., Aumont, O., DeAth, R., Dunne, J. P., Dutkiewicz, S., Galbraith, E., et al. (2016). How well do global ocean biogeochemistry models simulate dissolved iron distributions? *Global Biogeochemical Cycles*, *30*, 149–174. <https://doi.org/10.1002/2015GB005289>
- Taylor, S. R., & McLennan, S. M. (1995). The geochemical evolution of the continental crust. *Reviews of Geophysics*, *33*(2), 241–265. <https://doi.org/10.1029/95RG00262>
- Tonnard, M., Planquette, H., Bowie, A., van der Merwe, P., Gallinari, M., de Gésincourt, F. D., et al. (2020). Dissolved iron in the North Atlantic Ocean and Labrador Sea along the GEOVIDE section (GEOTRACES section GA01). *Biogeosciences*, *17*, 1–53. <https://doi.org/10.5194/bg-2018-147>
- Twining, B. S., & Baines, S. B. (2013). The trace metal composition of marine phytoplankton. *Annual Review of Marine Science*, *5*(1), 191–215. <https://doi.org/10.1146/annurev-marine-121211-172322>
- Twining, B. S., Baines, S. B., Bozard, J. B., Vogt, S., Walker, E. A., & Nelson, D. M. (2011). Metal quotas of plankton in the equatorial Pacific Ocean. *Deep-Sea Research Part II: Topical Studies in Oceanography*, *58*(3–4), 325–341. <https://doi.org/10.1016/j.dsr2.2010.08.018>
- Twining, B. S., Baines, S. B., & Fisher, N. S. (2004). Element stoichiometries of individual plankton cells collected during the Southern Ocean Iron Experiment (SOFEX). *Limnology and Oceanography*, *49*(6), 2115–2128. <https://doi.org/10.4319/lo.2004.49.6.2115>
- Twining, B. S., Rauschenberg, S., Morton, P. L., Ohnemus, D. C., & Lam, P. J. (2015). Comparison of particulate trace element concentrations in the North Atlantic Ocean as determined with discrete bottle sampling and in situ pumping. *Deep Sea Research, Part II*, *116*, 273–282. <https://doi.org/10.1016/j.dsr2.2014.11.005>



- Ussher, S. J., Achterberg, E. P., Powell, C., Baker, A. R., Jickells, T. D., Torres, R., & Worsfold, P. J. (2013). Impact of atmospheric deposition on the contrasting iron biogeochemistry of the North and South Atlantic Ocean. *Global Biogeochemical Cycles*, *27*, 1096–1107. <https://doi.org/10.1002/gbc.20056>
- Volk, T., & Hoffert, M. I. (1985). Ocean carbon pumps: Analysis of relative strengths and efficiencies in ocean-driven atmospheric CO<sub>2</sub> changes. In W. S. Broecker, & E. T. Sundquist (Eds.), *The carbon cycle and atmospheric CO<sub>2</sub>: Natural variations Archean to present* (pp. 99–110). Washington D. C: American Geophysical Union.
- Watson, A. J., Bakker, D. C. E., Ridgwell, A. J., Boyd, P. W., & Law, C. S. (2000). Effect of iron supply on Southern Ocean CO<sub>2</sub> uptake and implications for glacial atmospheric CO<sub>2</sub>. *Nature*, *407*(6805), 730–733. <https://doi.org/10.1038/35037561>
- Weinstein, S. E., & Moran, S. B. (2005). Vertical flux of particulate Al, Fe, Pb, and Ba from the upper ocean estimated from <sup>234</sup>Th/<sup>238</sup>U disequilibria. *Deep Sea Research, Part I*, *52*(8), 1477–1488. <https://doi.org/10.1016/j.dsr.2005.03.008>
- Westberry, T., Behrenfeld, M. J., Siegel, D. A., & Boss, E. (2008). Carbon-based primary productivity modeling with vertically resolved photoacclimation. *Global Biogeochemical Cycles*, *22*, GB2024. <https://doi.org/10.1029/2007GB003078>
- Winckler, G., Anderson, R., Fleisher, M., McGee, D., & Mahowald, N. (2008). Covariant glacial-interglacial dust fluxes. *Science*, *320*(5872), 93–96. <https://doi.org/10.1126/science.1150595>